Sigma J Eng & Nat Sci 38 (1), 2020, 289-303

Sigma Journal of Engineering and Natural Sciences
Sigma Mühendislik ve Fen Bilimleri Dergisi

Research Article

REMOVAL OF METHYLENE BLUE ON ZINC OXIDE NANOPARTICLES: NONLINEAR AND LINEAR ADSORPTION ISOTHERMS AND KINETICS STUDY

Shahin AHMADI[1], Chinenye Adaobi IGWEGBE*[2]

[1]*Department of Environmental Health, School of Public Health, Zabol University of Medical Sciences, Zabol, IRAN;* ORCID: 0000-0003-2831-2148
[2]*Department of Chemical Engineering, Nnamdi Azikiwe University, Awka, NIGERIA;*
ORCID: 0000-0002-5766-7047

Received: 06.11.2019 Revised: 19.12.2019 Accepted: 08.01.2020

ABSTRACT

Environmental pollution caused by colored effluents is threatening to the world. The aim of this study is to evaluate the applicability of Zinc oxide nanoparticles (ZnO-NPs) for the removal of methylene blue (MB) from aqueous solution and also to study the applicability of the nonlinear and linear adsorption isotherm and kinetic models on the process. The effects of various operating parameters such as pH (3 - 11), ZnO-NPs dosage (0.1 – 0.4 g/L), contact time (30 - 120 min), initial MB concentration (20 – 80 mg/L) on the removal of MB were studied. The adsorption kinetic and isotherm models were examined using the linear and nonlinear regression analyses methods. The results revealed that under optimal conditions of pH 7, ZnO-NPs dosage of 0.2 g/L and contact time of 60 min at concentration of 40 mg/L, the maximum adsorption capacity (q_m) of MB adsorption on ZnO NPs was 9.6. mg/g and maximum removal was 96.25 %. The MB adsorption data was found to follow the Langmuir isotherm model than the Freundlich model using the linear regression analysis method. But the values of the error functions (*RMSE, SD, RSS,* R^2_{adj}, and X^2_{red}) estimated revealed that the Freundlich isotherm was more suitable for describing the adsorption process. The process of MB adsorption on ZnO-NPs was found to be governed by the pseudo-second-order model using both the linear and nonlinear adsorption models. The rate-determining step is chemisorption. In general, the results indicated that the nonlinear fitting method of the experimental data with the models provided better results. The adsorption of MB on ZnO-NPs was favorable since the intensity of adsorption (n = 9.62) lies within the range of 1-10. The monolayer adsorption capacity (q_m) for ZnO-NPs with MB was 12.78 mg/g. It could be concluded from the study that ZnO-NPs can be useful for the removal of MB from its aqueous solution.
Keywords: Methylene blue, nanoparticles, kinetics, adsorption, error functions.

1. INTRODUCTION

Methylene blue dye-containing effluents from various industries such as textile, rubber, plastic, paper-making, printing, cosmetics, and food are established to be carcinogenic and also creates toxic effects on living organisms [1]. Colors are among the most dangerous chemicals found in industrial wastewater, which are imperative due to several reasons including diminished

* Corresponding Author: e-mail: ca.igwegbe@unizik.edu.ng, tel: +2348036805440

light permeability and impaired photosynthesis in water resources [2]. Methylene blue is a cationic color with a complex aromatic structure, which is used for coloring cotton and silk [3]. This compound can cause impaired respiration. Further, direct exposure to it causes permanent damage to the human and animal eyes; it also local burns, nausea and vomiting, mental disorders, and Methemoglobinemia [4, 5]. In addition, these compounds can cause negative effects on the appearance and quality of wa ter [6]. Therefore, wastewaters containing this dye were highlighted as one of the most important threatening in environmental and public health [7]. The aquatic ecosystem can also be affected due to the toxicity of these dyes [8].

Several treatment methods have been proposed for the removal of dyes from contaminated waters, which include photodecomposition [5, 9], electrolysis [6], adsorption [10-14], oxidation [15, 16] and other processes. Amongst the different physical and chemical processes, adsorption is an effective technique, which is successfully used for the removal of colors from wastewaters [17, 18]. The adsorption method is widely used due to its simplicity, low cost, and removal of color and other pollutants with great efficiency [19]. Adsorption can be either physisorption (which involves fairly weak intermolecular forces), or chemisorption (which involves basically the formation of a chemical bond between the sorbent molecule and the surface of the adsorbent [20]. Activated carbons have been used successfully to remove organic and mineral pollutants [13, 17] but they are hardly regenerated [7]. Nanoparticles are referred to as particles with a diameter of less than 100 nm [12]. Nanoparticles have been revealed to have a high potential in adsorbing organic compounds especially colors from wastewater and sewage tanks due to their high surface to volume ratio than other adsorbents [21]. ZnO is a basic oxide group and has been found to have a wide range of applications in the process of adsorption [22].

The main purpose of this study is to investigate the effectiveness of ZnO-NPs on the removal of MB from aqueous solution and the applicability of the nonlinear and linear adsorption isotherm and kinetic models on the process. The impact of various operating factors such as the contact time, adsorbent dosage, pH and initial MB concentration on the adsorption process will be studied to ascertain their optimum conditions.

2. MATERIALS AND METHODS

2.1. Materials

Methylene Blue (MB), a cationic dye with a molar mass of 319.85g/mol, molecular formula: $C_{16}H_{18}N_3CLS$, pKa:3.5 and wavelength of maximum absorption (λ_{max}):668nm was procured from Sigma-Aldrich Chemical Company (USA). Zinc oxide nanoparticles (ZnO-NPs) with a diameter of less than 20nm, purity of 99%, pKa of 7.5 and specific surface area of $90m^2/g$ were also purchased from Sigma-Aldrich Chemical Company (USA).

2.2. Structural characterization of ZnO NPs

X-ray diffraction (XRD) was used to define the structural features, diffractive arrangement and interplanar spacing of the ZnO-NPs (adsorbent) using an X-ray diffract meter with Philips PNA-analytical diffract meter. The morphology of ZnO-NPs was determined via scanning electron micro¬scopy (SEM). Fourier-transform infrared spectroscopy (FT-IR) of the adsorbent was done on a JASCO 640 plus machine (4000-400 cm^{-1}) at room temperature to determine the functional groups present in the adsorbent and taking part in the MB adsorption process.

2.3. Batch adsorption technique

All adsorption experiments were carried out at room temperature. The study was performed on a batch mode using the one-factor-at-a-time (OFAT) method. To carry out the experiments, a

stock solution of MB at a concentration of 1000 mg/L was prepared. The different concentrations of MB were prepared by dilution in deionized water (applying the relation: $C_1V_1=C_2V_2$). The effects of ZnO-NPs dosage (0.1-0.4 g/L), contact time (15-120 min), pH (3-11) and initial MB concentration (20-80 mg/L) on MB removal were investigated. At first, the effect of the pH (3, 5, 7, 8 and 11) on the process was studied at a contact time of 60 min by adding 0.1 g/L of ZnO-NPs to each beaker with 100 ml of the MB solution with an initial MB concentration of 60 mg/L. The pH of the solution was adjusted using 0.1N HCl or 0.1N NaOH solutions. The beaker with its contents was placed on a shaker and rotated at a speed of 180 rpm. After a specific time of contact, the samples were filtered using the Whatman filter paper (size: 40μm). The residual MB concentration of the filtrate was measured to determine the adsorption capacity and removal efficiency. The optimum dosage of the adsorbent was determined at a contact time of 60 min, MB initial concentration of 60 mg/L at the optimum pH obtained. Also, the effect of initial MB concentration was studied by varying the contact time at the optimum pH and optimum ZnO-NPs dosage. The residual concentrations were measured using a UV-visible spectrophotometer (MODEL: LUV-100A). The amount of MB adsorbed on ZnO-NPs (q_e) was evaluated using Eq. (1):

$$q_e = \frac{(C_0 - C_e)V}{M} \tag{1}$$

Also, the removal efficiency (*%R*) was calculated based on Eq. (2) [23-26]:

$$\%R = \frac{(C_0 - C_f)}{C_0}100 \tag{2}$$

Where C_0 (mg/L) is the initial concentration of MB and C_e (mg/L) is the equilibrium liquid phase concentration of MB, C_f (mg/L) is the final concentration, V is the volume of the solution (L) and M is the amount of ZnO-NPs used (g).

3. RESULTS AND DISCUSSION

3.1. XRD, SEM and FTIR analysis on ZnO-NPs

The XRD result (Figure 1a) indicates that the ZnO-NPs possess a crystalline structure. This crystalline structure increases the adsorption, where the adsorbate is adsorbed on the upper layer of the crystalline structure of the adsorbent surface by means of physisorption [27]. The XRD image also showed that the maximum peak is around $2\theta=36^0$ with very high intensity. The surface morphology of ZnO-NPs is shown in Figure 1b. The ZnO particles look lamellar-like in arrangement. The specific surface area is one of the parameters determining the adsorption capability of an adsorbent [28]. Figure 1b also shows that the NPs are highly porous in nature which indicates the presence of high surface area which will lead to a higher level of contact with the adsorbate, MB [28]. A plot of the infrared transmittance (%) against the wavelength (cm^{-1}) can be seen in Figure 1c. The FTIR analysis on the ZnO-NPs indicates the existence of C–O stretch of alcohols, carboxylic acids, esters, ethers (1097.08 cm^{-1}) and C–H rock of alkanes (1384.50 cm^{-1}). The peaks 1638.09 and 1617.65 cm^{-1} show the presence of C–C stretch (in-ring) of aromatics. Peak 2925.73 cm^{-1} indicates the existence of C–H stretch alkanes, which are strong, broad and multi-banded. The presence of O–H stretch, H–bonded of alcohols, phenols (3415.78 cm^{-1}), which are also strong and broad bands can be observed. The O–H bands are very important sites for adsorption [29]. The hydroxyl group effect is more felt due to the hydrogen bonding with other hydroxyl bonds since they do not exist in isolation establishing a stable structure [28, 29].

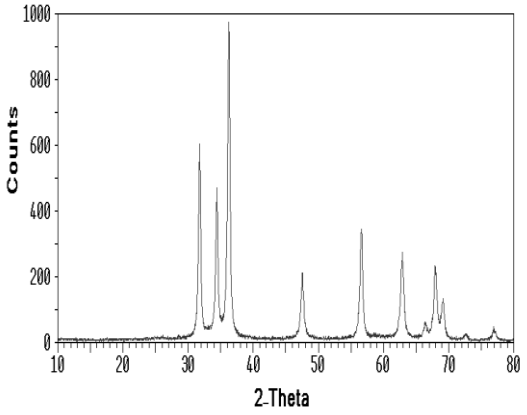

(a)

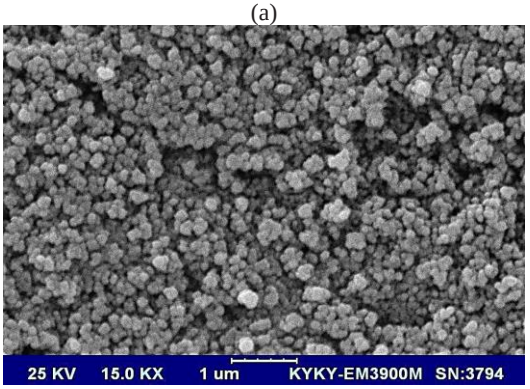

(b)

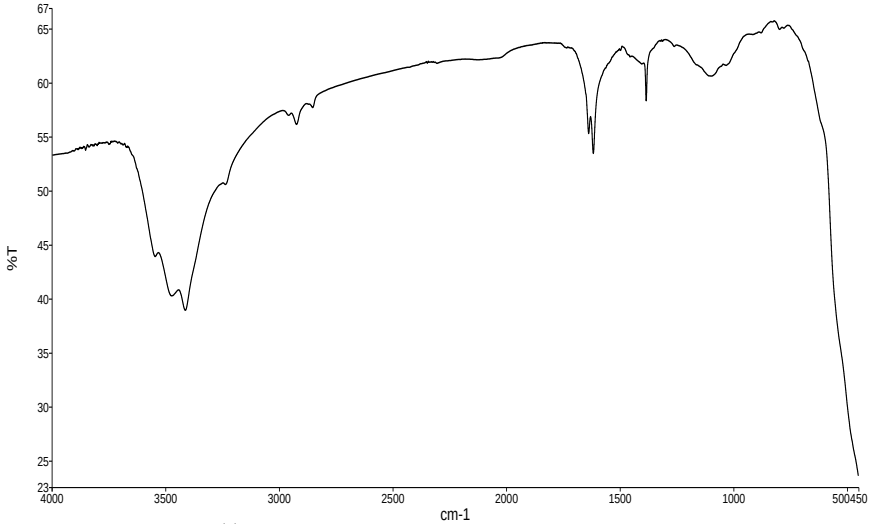

(c)

Figure 1. (a) XRD, (b) SEM image, and (c) FTIR spectra of ZnO-NPs

3.2. Effect of pH

The influence of pH (3-11) on adsorption of MB using ZnO-NPs was studied at a time of 60 min, initial MB concentration of 60 mg/L, and ZnO-NPs dosage of 0.1 g/L. Figure 2 shows that the percentage removal of MB increased from 92.16 to 93.3 % as the pH was increased from 3 to 7; the amount of MB adsorbed also increased from 27.65 to 28 mg/g. The solution pH is one of the parameters affecting the adsorbent level and ionization of pollutants. The influence of pH depends on the point zero charge (pHzpc) of the catalyst and acidity constant (pKa). MB has a pKa value of 3.5, and pHzpc value for ZnO-NPs is 7.5 [25, 30]. At pH higher than these values, MB and ZnO-NPs had a negative charge. Therefore, the force between them will be repulsive, and they will have no tendency to react. Thus, MB removal declined at alkaline pH values. At pH values below 7.5, ZnO-NPs surface had a positive charge and thus possesses a greater adsorption force, causing greater MB removal [31].

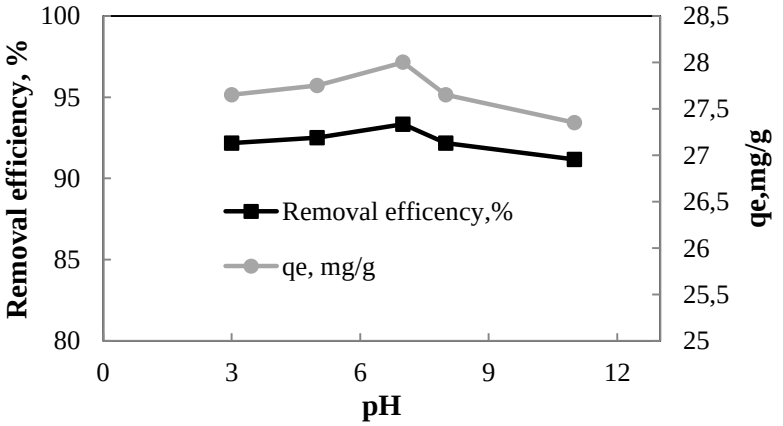

Figure 2. Effect of pH on removal efficiency of MB (Time: 60 min, ZnO-NPs dosage: 0.1 g/L, initial MB concentration: 60 mg/L).

3.3. Effect of adsorbent dosage

The effect of ZnO-NPs dosage on MB removal was studied by varying the dosage from 0.1 to 0.4 g/L at an initial MB concentration of 60 mg/L and a pH of 7. Figure 3 shows that the removal efficiency was enhanced as the dosage was increased from 0.1 to 0.2 g/L. Maximum removal efficiency occurred at a dosage of 0.2 g/L (97.5 %). The amount of MB adsorbed on ZnO-NPs (q_m) at the dosage of 0.2 g/L was 21 mg/g. This may be owed to the increase in the number of active sites available for MB adsorption [32]. The removal efficiency was decreased as the adsorbent dosage was increased above 0.2 g/L, which may be due to the fact that as the amount of adsorbent is increased, the total surface area available for the adsorption of MB diminishes as a result of overlapping or aggregation of adsorption sites [33, 34].

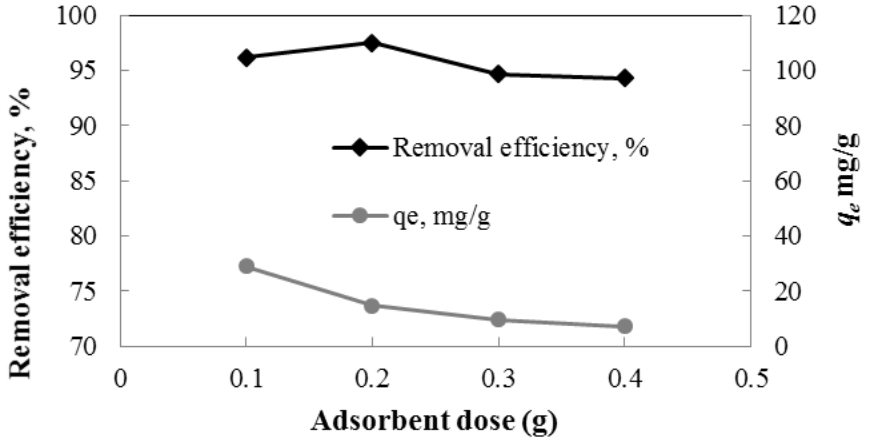

Figure 3. Effect of adsorbent dosage on removal efficiency of MB (Time: 60 min, pH: 7, initial MB concentration: 60 mg/L).

3.4. Effect of initial MB concentration

Figure 4 shows the effect of initial MB concentration (20–80 mg/L) on the removal of MB on ZnO-NPs. The adsorption capacity increased and the removal efficiency decreased with increasing MB concentration. The dye was adsorbed on the outer surface of the adsorbent; after complete adsorption on the outer surface, the dye entered into the inner surface through the pores [35, 36]. The adsorption efficiency decreased as the initial concentration of MB increased from 40 to 80 mg/L because of the decrease in the active sites [25]. The reduction in the efficiency by increasing the concentration of pollutants can be expressed by the constant of other parameters effective against the increase of pollutant concentration, and the filling of active nanoparticles sites by pollutants in the process. Other researchers also confirmed that as the initial concentration of the pollutant was increased, the removal efficiency was decreased [37].

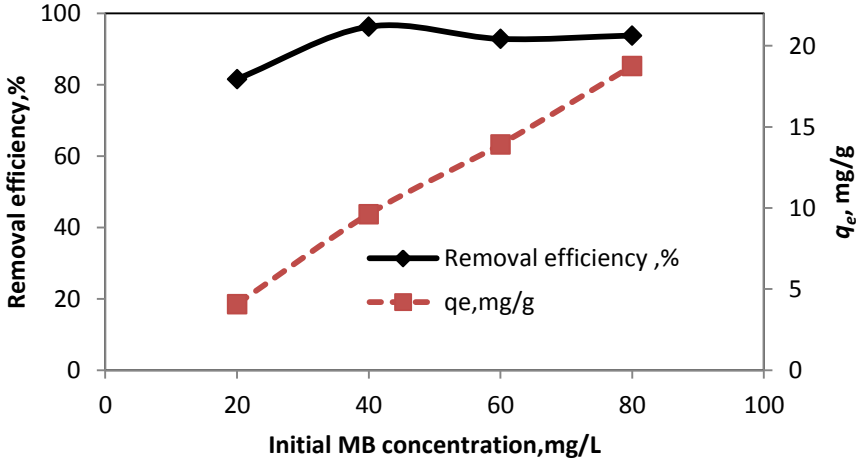

Figure 4. Effect of initial MB concentration on removal efficiency of MB (Time: 60 min, pH: 7, dosage: 0.2g/L).

3.5. Effect of contact time

The effect of contact time on the MB adsorption process was investigated by varying the contact time from 30 to 120 min using ZnO-NPs dosage of 0.2 g/L and MB concentration of 40 mg/L at pH of 7. Figure 5 shows the effect of contact time on the removal of MB on ZnO-NPs. The MB adsorption was increased with increasing the time of contact from 30 to 60 min and reached equilibrium at 60 min. This was due to the increase in the period of contact between the adsorbent and the adsorbate [32]. But as the time of treatment was increased beyond 60 min, the percentage of MB adsorbed decreased. After 60 min, desorption took place [38].

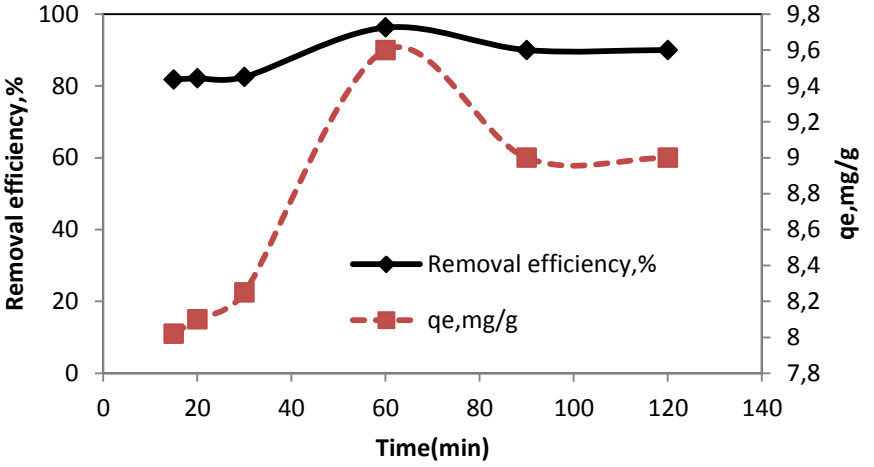

Figure 5. Effect of contact time on removal efficiency of MB (ZnO-NPs dosage: 0.2 g/L; pH: 7, initial MB concentration: 40 mg/L).

3.6. Adsorption isotherms and kinetics

The Langmuir and Freundlich isotherms are the two well-known adsorption isotherm models. These isotherms were used in this study to determine the relationship between the amount of dye adsorbed and its equilibrium concentration in solution. For the isotherm study, 0.2 g/L ZnO-NPs were added to the MB solution with a concentration of 40 mg/L at pH 7 and stirred for 60 min.

Adsorption kinetic models are used to examine the rate of adsorption process and the potential rate-controlling step. To determine the kinetic order and the time required to reach adsorption equilibrium, the adsorption kinetic study of MB on ZnO-NPs biomass was carried out at room temperature. The adsorption kinetics experiment was carried out using ZnO-NPs dosage of 0.2 g/L, MB concentration of 40 mg/L, pH 7 at different contact times (15, 20, 30 60, 90, and 120 min).

The different isotherm and kinetics equations (linear and nonlinear equations) are presented in Table 1 [12, 39-41]. Where q_e (mg/g) and q_t (mg/g) are the amounts of MB adsorbed at equilibrium and at time t, respectively; q_m (mg/g) is the maximum or monolayer adsorption capacity, and C_e is the equilibrium concentration of MB in the solution (mg/L); k_1 (/min) is the pseudo-first-order rate constant of adsorption, K_2 (g mg/min) is the pseudo-second-order rate constant, and K_L (L/mg) is the Langmuir isotherm constant related to the affinity of the binding sites and energy of adsorption; K_F (mg/g)(L/mg) and n are the constants incorporating the factors affecting the adsorption capacity and intensity of adsorption, respectively.

Table 1. The equation of isotherms and kinetics.

Isotherm and kinetic type	Main equation (nonlinear)	Linear form
Freundlich	$q_e = K_F C_e^{1/n}$	$Logq_e = {}^{1}/_{n}\, LogC_e + LogK_F$
Langmuir	$q_e = \frac{q_m K_L C_e}{1 + K_L C_e}$	${}^{C_e}/_{q_e} = {}^{1}/_{q_m K_L} + {}^{C_e}/_{q_m}$
Pseudo-first-order	$q_t = q_e(1 - \exp(-k_1 t))$	$Log(q_e - q_t) = Logq_e - \frac{k_1}{2.303} t$
Pseudo-second-order	$q_t = \frac{q_e^2}{1 + q_e K_2 t}$	${}^{t}/_{q_t} = {}^{1}/_{K_2 q_e^2} + {}^{t}/_{q_e}$

In order to further validate the adsorption mathematical models (nonlinear isotherm and kinetic models) with the experimental results, a number of error functions were used, which are available in the literature. The use of only the R^2 for the validation of nonlinear isotherm and kinetic data analysis is not sufficient enough, because the experimental results may have high R^2 value. Therefore, it is necessary to diagnose the result of regression for residue analysis. In this study, five types of statistical functions were used in this study. The different error functions equations used to validate the nonlinear isotherm and kinetic models are presented in Table 2 [40, 42-44]. Where *N* is the number of performed experiments, *P* is the number of parameters of the fitted model, q_c is the value that is calculated from the model fit, q_e is calculated from test elements and *p* is the number of test element and R^2 is the coefficient of determination.

Table 2. The equations of error functions.

Isotherm and kinetic type	Equation
Standard deviation (*SD*)	$SD = \sqrt{\left(\frac{1}{N-P}\right)\sum_{i=1}^{N}\left(q_{i,observed} - q_{i,calculated}\right)^2}$
The coefficient of determination (R^2)	$R^2 = \left[\frac{\sum_{i=1}^{N}\left(q_{i,observed} - \bar{q}_{observed}\right) - \sum_{i=1}^{N}\left(q_{i,observed} - q_{i,cal}\right.}{\sum_{I=1}^{N}\left(q_{i,observed} - \bar{q}_{observed}\right)^2}$
Adjusted R-squared ($\boldsymbol{R^2_{adj}}$)	$R^2_{adj} = 1 - (1 - R^2)\left(\frac{N-1}{N-P-1}\right)$
Reduced Chi-squared ($\boldsymbol{X^2_{red}}$)	$X^2_{red} = \sum_{1=1}^{N}\frac{\left(q_{i,observed} - q_{i,calculated}\right)^2}{N-P}$
Residual sum of squares (*RSS*)	$RSS = \sum_{I=1}^{N}\left(q_{i,observed} - q_{i,calculated}\right)$
Root-mean-square error (*RMSE*)	$RMSE = \sqrt{\frac{1}{p-2}\sum_{i=1}^{p}(q_e - q_c)^2}$

The linear adsorption isotherm and kinetics plots are shown in Figures 6 and 7. The estimated linear isotherm and kinetics parameters and their respective correlation coefficients, R^2 are presented in Table 3. The MB adsorption experimental data was found to conform more to the pseudo-second-order kinetic model (with R^2 = 0.9974) than the pseudo-first-order model (R^2 =

0.7029), which suggests a chemisorption process [8, 45]. It is found that the Freundlich model (R^2 = 0.9384) is more suitable to satisfactorily describe the studied sorption phenomenon than the Langmuir (R^2 = 0.9368) model using the linear forms of the isotherm equations.

The estimated nonlinear isotherm and kinetics parameters and their respective correlation coefficients, R^2 are presented in Table 4. A lower value of *RMSE* shows a better fit. The higher values of R^2 and lower values of *RMSE*, *SD*, R^2_{adj}, and X^2_{red} imply that the pseudo-second-order kinetic model best explained the studied adsorption process. The estimated nonlinear isotherm parameters, fixed correlation coefficient (R^2), *RMSE* and the other error analysis functions are presented in Table 4. Considering the error range for each model, it was deduced that the Langmuir and Freundlich models were adequate for describing the adsorption process. But the MB adsorption equilibrium data conformed more to the Langmuir isotherm compared to the Freundlich isotherm with regards to its correlation coefficient, R^2 (Table 4). Langmuir isotherm indicates the surface homogeneity of the adsorbent [46]. In fact, by comparing the values of the error functions, the Freundlich was found to be the more suitable model for the description of the adsorption of MB on ZnO-NPs with the lowest values of *RMSE*, *RSS*, *SD*, R^2_{adj}, and X^2_{red}. The Freundlich adsorption model assumes a heterogeneous surface [46].

Generally, the results (shown in Tables 3 and 4) indicated that the nonlinear method of regression analysis provided better results based on fitting the experimental data with the isotherm and kinetic models studied. Also, *n* (the intensity of adsorption) was determined as 9.62, which lies within the range of 1 to 10 suggesting that the adsorption of MB on ZnO-NPs is favorable [47]. The monolayer adsorption capacity (q_m) for ZnO-NPs with MB was 12.78 mg/g.

Table 3. Parameters of linear isotherm and kinetics for MB adsorption on ZnO-NPs.

Freundlich		Langmuir	
K_F	10.21	K_L	0.3916
n	9.43	q_m	21.79
R^2	0.9384	R^2	0.9368
Pseudo-first-order		Pseudo-second-order	
k_1	0.00276	K_2	0.06089
q_e	1.3089	q_e	9.225
R^2	0.7029	R^2	0.9974

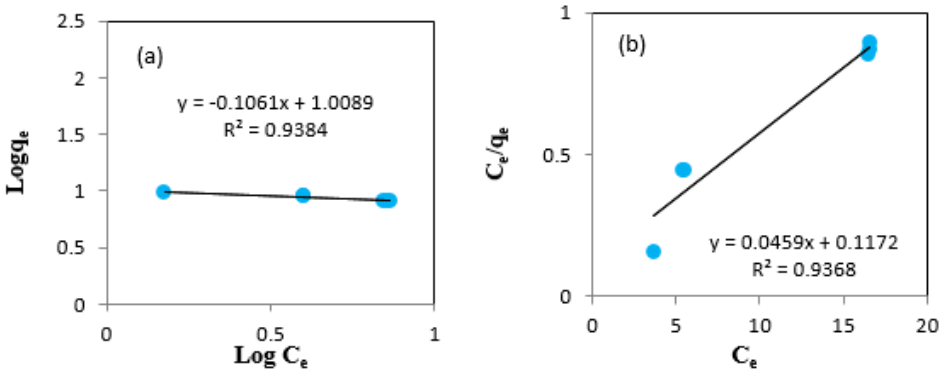

Figure 6. Linear (a) Freundlich, (b) Langmuir model plots of MB adsorption on ZnO-NPs.

Table 4. Parameters of nonlinear isotherm and kinetics for MB adsorption on ZnO-NPs.

Freundlich		Langmuir	
K_F	11.13	K_L	12.5
n	9.62	q_m	12.78
RSS	0.058	RSS	0.031
X^2_{red}	0.0149	X^2_{red}	0.006
SD	0.0123	SD	0.081
R^2	0.9654	R^2	0.988
R^2_{adj}	0.92	R^2_{adj}	0.934
RMSE	0.32	RMSE	0.47
Pseudo-first-order		Pseudo-second-order	
k_1	0.0012	K_2	0.023
$q_{e(cal)}$	9.6	$q_{e(cal)}$	24
RSS	0.002	RSS	0.004
X^2_{red}	0.0019	R^2_{adj}	0.00039
SD	0.022	SD	0.021
R^2	0.91	R^2	0.995
R^2_{adj}	0.921	R^2_{adj}	0.993
RMSE	0.46	RMSE	0.42

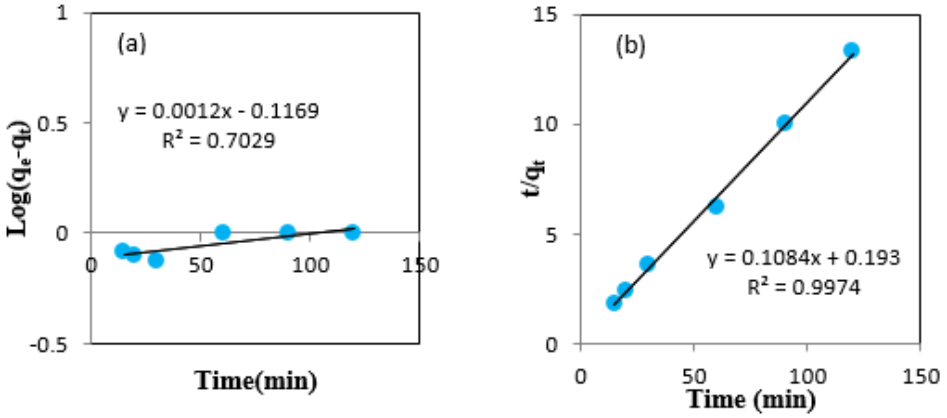

Figure 7. Linear (a) pseudo-first-order, (b) pseudo-second-order plots of MB adsorption on ZnO-NPs.

The comparison of ZnO NPs with other adsorbents for methylene blue removal

The removal efficiencies (*%R*) of methylene blue (MB) using various adsorbents are listed in Table 5. Table 5 reveals that ZnO-NPs is a capable material that can be used for the removal of MB from water containing MB when compared with the other adsorbents. Table 5 also proves that methylene blue, a cationic dye can be removed from effluents using the adsorption technique via different adsorbent materials.

Table 5. Comparison of ZnO-NPs with other adsorbents for the removal of MB.

Adsorbent material	Maximum removal efficiency	Conditions	Reference
Sulfuric acid–treated orange peel	100 %	pH: 8 Adsorbent dose: 0.4 g/L Contact time: 45 min MB concentration: 50 mg/L Temperature: 30 ^{0}C Volume of solution: 100 mL	[1]
Biochar from hazelnut shell	83 %	pH: 4.0 adsorbent dosage: 1.5g/L Contact time: 300 min initial dye concentration: 15 mg/L Temperature: 45 ^{0}C Agitation speed: 150 rpm Volume of solution: 250 mL	[48]
Luffa adsorbent modified with sodium dodecyl sulfate anionic surfactant	99 %	pH: 6 Adsorbent dose: 1 g Contact time: 60 min MB concentration: 50 mg/L Temperature: 25 ^{0}C Agitation speed: 115 rpm Volume of solution: 100 cc	[49]
Activated carbon derived from corn stalk (AC-CS)	90 %	pH: 11 AC-CS dose: 1.4 g/L Contact time: 50 min MB concentration: 10 mg/L Temperature: 25 ± 2 °C Volume of solution: 100 mL	[50]
$HoCaWO_4$ nanoparticles	71.17 %	pH: 2.03 nanoparticles dose: 1.91 g/L Contact time: 15.16 min MB concentration: 100.65 mg/L Agitation speed: 180 rpm Temperature: 25 ± 2 °C Volume of solution treated: 100 mL	[11]
Modified pumice stone	84.8 %	pH: 10 nanoparticles dose: 0.2 g/L Contact time: 120 min MB concentration: 30 mg/L Volume of solution treated: 50 cc	[51]
Silica derived from the raw rice husk	96.7%	pH: 8 Adsorbent dose: 1 g/L Contact time: 60 min MB concentration: 10 mg/L Volume of solution treated: 100 mL	[52]
Orange (*Citrus sinensis*) peels biochar (OPBC)	99 %	pH: 5.6 OPAC dosage: 0.16 g/L Contact time: 100 min MB concentration: 50 mg/L Temperature: 333 K Agitation speed: 110 stroke/min Volume of solution treated: 200 mL	[46]

Zinc oxide nanoparticles (ZnO-NPs)	96.25 %	pH: 7 ZnO-NPs dose: 0.2 g/L Contact time: 60 min MB concentration: 40 mg/L Temperature: 25 ± 2 °C Agitation speed: 180 rpm Volume of solution treated: 100 mL	This study

4. CONCLUSIONS

Zinc oxide nanoparticles (ZnO-NPs) were applied for the removal of methylene blue (MB) dye from aqueous solution using the adsorption process. In this study, the ZnO-NPs was characterized using the XRD, SEM and FTIR analyses. The operating parameters affecting the adsorption capacity were investigated including contact time, initial concentration, pH of the solution and ZnO-NPs dosage. The comparison of the nonlinear and linear regression methods on the adsorption kinetics and isotherm models were done to reveal the models which best described the adsorption of MB on ZnO-NPs. The characterization results revealed that the ZnO-NPs can be used for the removal of MB. The maximum adsorption capacity (q_m) of MB adsorption on ZnO-NPs was 9.6 mg/g and maximum removal efficiency was 96.25 %. These were achieved at optimum conditions of the initial concentration of 40 mg/L, pH of 7, ZnO-NPs dosage of 0.2 g/L and contact time of 60 min. The results showed that equilibrium was reached at 60 min. Also, the MB adsorption on ZnO-NPs followed the pseudo-second-order kinetic model than the pseudo-first-order kinetic model using both the linear and nonlinear regression methods. The experimental data were found to fit into the Langmuir isotherm model than the Freundlich model using the linear regression method, but by using the nonlinear regression analysis, the Freundlich best described the removal process. The adsorption process was also found to be favorable. Generally, the results indicated that the nonlinear fitting method of the experimental data with the isotherm and kinetic models provided better results. The monolayer adsorption capacity (q_m) for ZnO-NPs with MB was 12.78 mg/g. Based on the data obtained from the present study, it can be concluded that adsorption by ZnO-NPs is an efficient and reliable method for methylene blue (MB) removal from liquid solutions. Since simulated methylene blue wastewater was used in the present study, further studies can be done on real methylene blue-containing effluent.

Acknowledgments

The authors wish to thank the Zabol University of Medical Sciences, Iran for their financial support.

REFERENCES

[1] Kumar P.S., Fernando P.S.A., Ahmed R.T., Srinath R., Priyadharshini M., Vignesh A.M., Thanjiappan A., (2014) Effect of temperature on the adsorption of methylene blue dye onto sulfuric acid–treated orange peel, *Chemical Engineering Communication* 11, 1526-1547.

[2] Royer B., Cardoso N.F., Lima E.C., Macedo T.R., Airoldi C., (2010) A useful organ functionalized layered silicate for textile dye removal, *Journal of Hazardous Materials* 181, 366-374.

[3] Srivastava S.N., (2008) Effects of process variables on kinetics of methylene blue sorption onto untreated guava (Psidium guajava) leaf powder: Statistical analysis, *Chemical Engineering Journal* 140, 609-621.

[4] Rafatullah M., Sulaiman O., Hashim R., Ahmad A., (2010) Adsorption of methylene blue on low-cost adsorbents: A review, *Journal of Hazardous Materials* 177, 70-78.

[5] Mulugeta M., Belisti L., (2014) Removal of methylene blue (MB) dye from aqueous solution by bioadsorption onto untreated Parthenium hystrophorous weed, *Modern Chemistry Applications* 2, 1-5.

[6] Qingdong Q., Sun T., Yin W., Xu Y., (2017) Rapid and efficient removal of methylene blue by freshly prepared manganese dioxide, *Cogent Engineering* 1, 1-10.

[7] Ahmadi S., Kord Mostafapour F., (2017) Adsorptive removal of aniline from aqueous solutions by *Pistacia atlantica* (Baneh) shells: isotherm and kinetic studies, *Journal of Science, Technology and Environment Informatics* 5, 327–335.

[8] Igwegbe C.A., Onyechi P.C., Onukwuli O.D., Nwokedi I.C., (2016) Adsorptive treatment of textile wastewater using activated carbon produced from *Mucuna pruriens* seed shells, *World Journal of Engineering and Technology* 4, 21-37.

[9] Kapdan I.K., Kargi F., (2002) Simultaneous biodegradation, and adsorption of textile dye stuff in an activated sludge unit, *Process Biochemistry* 37, 973-98.

[10] Ahmadi Sh., Kord Mostafapoor F., (2017) Adsorptive removal of bisphenol A from aqueous solutions by *Pistacia atlantica:* isotherm and kinetic studies, *Pharmaceutical and Chemical Journal* 4, 1–8.

[11] Igwegbe C.A., Mohmmadi L., Ahmadi S., Rahdar A., Khadkhodaiy D., Dehghani R., Rahdar S., (2019) Modeling of adsorption of Methylene blue dye on Ho-CaWO4 nanoparticles using Response surface methodology (RSM) and Artificial neural network (ANN) techniques, *MethodsX* 6, 1779-1797.

[12] Igwegbe C.A., Banach A.M., Ahmadi S., (2018) Adsorption of Reactive Blue 19 from aqueous environment on magnesium oxide nanoparticles: kinetic, isotherm and thermodynamic studies, *Pharmaceutical and Chemical Journal* 5, 111-121.

[13] Igwegbe C.A., Onyechi P.C., Onukwuli O.D., (2015) Kinetic, isotherm and thermodynamic modelling on the adsorptive removal of malachite green on *Dacryodes edulis* seeds, *Journal of Scientific and Engineering Research* 2, 23-39.

[14] Ahmadi S., Rahdar A., Rahdar S., Igwegbe C.A., (2019) Removal of Remazol Black B from aqueous solution using P-γ-Fe_2O_3 nanoparticles: synthesis, physical characterization, isotherm, kinetic and thermodynamic studies, *Desalination and Water Treatment* 152, 401–410.

[15] Ahmadi S, Mohammadi L, Igwegbe C.A., Rahdar S., Banach A.M., (2018) Application of response surface methodology in the degradation of Reactive Blue 19 using H_2O_2/MgO nanoparticles advanced oxidation process, *International Journal of Industrial Chemistry* 9(3), 241-253.

[16] Ahmadi S., Igwegbe C.A., Rahdar S., (2019) The application of thermally activated persulfate for degradation of Acid Blue 92 in aqueous solution, *International Journal of Industrial Chemistry* 10(3), 249–260.

[17] Han Y., Quan X., Chen S., Zhao H., Cui C., Zhao Y., (2006) Electro-chemically enhanced adsorption of aniline on activated car-bon fibers, *Separation and Purification Technology* 50, 365–372.

[18] Sarvani R., Damani E., Ahmadi Sh., (2018) Adsorption isotherm and kinetics Study: Removal of phenol using adsorption onto modified *Pistacia mutica* shells, *Iranian Journal of Health Sciences* 6, 33-42.

[19] Samadi M.T., Kashitarash E.Z., Ahangari F., Ahmadi Sh., Jafari J., (2013) Nickel removal from aqueous environments using carbon nanotubes, *Water and Wastewater* 24, 38–44.

[20] Karine S.C., (2001) Adsorption kinetics of dyes and yellowing inhibitors on pulp fibers, 0885-0885.

[21] Rahdar S., Igwegbe C.A., Rahdar A., Ahmadi S., (2018) Efficiency of sono-nano-catalytic process of magnesium oxide nanoparticle in removal of penicillin G from aqueous solution, *Desalination and Water Treatment* 106, 330–335.

[22] Hong R., Pan T., Qian J., Li H., (2006) Synthesis and surface modification of ZnO nanoparticles, *Chemical Engineering Journal* 119, 71-81.

[23] Ahmadi Sh, Kord Mostafapour F., Bazrafshan E., (2017) Removal of aniline and from aqueous solutions by coagulation/flocculation flotation, *Chemical Science International Journal* 18, 1–10.

[24] Ahmadi Sh., Kord Mostafapour F., (2017) Survey of efficiency of dissolved air flotation in removal penicillin G potassium from aqueous solutions, *British Journal of Pharmaceutical and Medical Research* 15, 1–11.

[25] Bazrafshan E, Ahmadi Sh., (2017) Removal COD of landfill leachate using coagulation and activated tea waste ($ZnCl_2$) adsorption, *International Journal of Innovative Science Engineering and Technology* 4, 339-347.

[26] Rahdar S., Samani S., Ahmadi Sh., (2018) Efficiency of *Arachis hypogaea* ash in aniline adsorption from aqueous solution: a thermodynamic and kinetic study, *Journal of Health Research in Community* 4, 21-32.

[27] Elnasri, N.A., Elsheik, M.A., & Eltayeb M.B. (2013). Physico-chemical characterization and Freundlich isotherm studies of adsorption of Fe(II), from aqueous solution by using activated carbon prepared from Doumfruit waste. Archives of Applied Science Research, 5, 149-158.

[28] Okeola O.F., Odebunmi E.O., Ameen O.M., (2012) Comparison of sorption capacity and surface area of activated carbon prepared from Jatropha curcas fruit pericarp and seed coat, *Bulletin of the Chemical Society of Ethiopia* 2, 171-180.

[29] Coates J., (2010) Interpretation of Infrared Spectra. A Practical Approach. Encyclopedia of Analytical Chemistry. R.A. Meyers (ed.): John Wiley & Sons Ltd, Chichester, 10815–10837, 2010.

[30] Bonetto L.R., Ferrarini F., De Marco C., Crespo J.S., Guégan R., Giovanela M., (2015) Removal of methyl violet 2B dye from aqueous solution using a magnetic composite as an adsorbent, *Journal of Water Process Engineering* 6, 11-20.

[31] Ertas M., Acemioglu B., Alma M.H., Usta M., (2010). Removal of methylene blue from aqueous solution using cotton stalk, cotton waste and cotton dust, *Chemical Engineering Journal* 183, 421-427.

[32] Ahmadi Sh., Banach A., Kord Mostafapour F., Balarak D., (2017) Study survey of cupric oxide nanoparticles in removal efficiency of ciprofloxacin antibiotic from aqueous solution: adsorption isotherm study, *Desalination and Water Treatment* 89, 297–303.

[33] Nsami J.N, Mbadcam J.K., (2013) The adsorption efficiency of chemically prepared activated carbon from cola nut shells by $ZnCl_2$ on methylene blue, *Journal of Chemistry*, 1-7.

[34] Das B, Mondal N.K., (2011) Calcareous soil as a new adsorbent to remove lead from aqueous solution: equilibrium, kinetic and thermodynamic study, *Universal Journal of Environmental Research and Technology* 4, 515–530.

[35] Chakravarty P., Sarma N.S., Sharma H.P., (2010) Removal of Pb (II) from aqueous solution using heartwood of Areca catechu powder, *Desalination* 256, 16-21.

[36] Ata S., Din M.I., Rasool A., Qasim I., Ul Mohsin I., (2012) Equilibrium, thermodynamics, and kinetic sorption studies for the removal of coomassie brilliant blue on wheat bran as a low cost adsorbent, *Journal of Analytical Methods in Chemistry*, 1-8.

[37] Calvete T., Lima E.C., Cardoso N.F., Silvio L.D., Pavan F.A., (2009) Application of carbon adsorbents prepared from the Brazilian-pine fruit shell for removal of procion red MX 3B from aqueous solution-kinetic, equilibrium and thermodynamic studies, *Chemical Engineering Journal* 155, 627–636.

[38] Rahdar S., Ahmadi Sh., (2016) Removal of phenol and aniline from aqueous solutions by using adsorption onto *Pistacia terebinthus*: study of adsorption isotherm and kinetics, *Journal of Health Research in Community* 2, 35–45.

[39] Igwegbe C.A., Al-Rawajfeh A.E., Al-Itawi H.I., Al-Qazaqi S., Hashish E.A., Al-Qatatsheh M., Sharadqah S., Sillanpaa M., (2019) Utilization of calcined gypsum in water and wastewater treatment: removal of phenol, *Journal of Ecological Engineering* 20(7), 1–10.

[40] Ahmadi S., Igwegbe C.A., Rahdar S., Asadi Z., (2019) The survey of application of the linear and nonlinear kinetic models for the adsorption of nickel (II) by modified multi-walled carbon nanotubes, *Appl. Water Sci.* 9, 98.

[41] Ahmadi S., Igwegbe C.A., (2018) Adsorptive removal of phenol and aniline by modified bentonite: adsorption isotherm and kinetics study, *Applied Water Science* 8:170.

[42] Carneiro P.A., Umbuzeiro G.A., Oliveira D.P., Zanoni M.V.B., (2010) Assessment of water contamination caused by a mutagenic textile effluent/dyehouse effluent bearing disperse dyes, *Journal of Hazardous Materials* 174, 694-699.

[43] Khoshnamvand N., Ahmadi Sh., Kord Mostafapour F., (2017) Kinetic and isotherm studies on Ciprofloxacin an adsorption using magnesium oxide nanoparticles, *Journal of Applied Pharmaceutical Science* 7, 079-083.

[44] Jokiniemi J., Naushad M., Bhatnagar A., (2017) Optimization of fluoride removal from aqueous solution by Al2O3 nanoparticles, *Journal of Molecular Liquids* 238, 254–262.

[45] Igwegbe C.A., Onukwuli O.D., Nwabanne J.T., (2016) Adsorptive removal of vat yellow 4 on activated *Mucuna pruriens* (velvet bean) seed shells carbon, *Asian Journal of Chemical Sciences* 1, 1-16.

[46] Jawad A., Al-Heetim D., Abd Rashid R., (2019). Biochar from orange (*Citrus sinensis*) peels by acid activation for methylene blue adsorption, *Iranian Journal of Chemistry and Chemical Engineering* 38(2), 91-105.

[47] Rahdar S., Rahdar A., Igwegbe C.A., Moghaddam F., Ahmadi S., (2019) Synthesis and physical characterization of nickel oxide nanoparticles and its application study in the removal of ciprofloxacin from contaminated water by adsorption: Equilibrium and kinetic studies, *Desalination and Water Treatment* 141, 386–393.

[48] Kaya N., Yıldız Z. ve Ceylan S., (2018) Preparation and characterisation of biochar from hazelnut shell and its adsorption properties for methylene blue dye, *Politeknik Dergisi* 21(4), 765-776.

[49] Abbasi H., Asgari H., (2018) Removal of methylene blue from aqueous solutions using Luffa adsorbent modified with sodium dodecyl sulfate anionic surfactant, *Global NEST Journal* 20(3), 582-588.

[50] Nayeri D., Mousavi S.A., Fatahi M., Almasi A., Khodadoost F., (2019) Dataset on adsorption of methylene blue from aqueous solution onto activated carbon obtained from low cost wastes by chemical-thermal activation e modelling using response surface methodology, *Data in Brief* 25, 104036.

[51] Derakhshan Z., Baghapour M.A., Ranjbar M., Faramarzian M, (2013) Adsorption of methylene blue dye from aqueous solutions by modified pumice stone: kinetics and equilibrium studies, *Health Scope* 2(3), 136-144.

[52] Moeinian K., Mehdinia S.M., (2019) Removing Methylene Blue from aqueous solutions using rice husk silica adsorbent, *Pol. J. Environ. Stud.* 28(4):2281–2287.